A Comprehensive Approach for Analytical Modeling of Line Commutated Converter based Multiterminal HVDC Systems

Markus Blechschmidt, Christoph Hahn, *Member*, *IEEE*, Matthias Luther, *Member*, *IEEE*
Institute of Electrical Energy Systems, Friedrich-Alexander-University Erlangen-Nuremberg (FAU), Germany
markus.mb.blechschmidt@fau.de, christoph.hahn@fau.de, matthias.luther@fau.de

***Abstract*— This paper presents an analytical model of Line Commutated Converter (LCC) based Multiterminal (MT) High-Voltage Direct Current (HVDC) systems. The approach is based on space phasor transformation and provides a modular HVDC model, since every converter of the MT system is carried out as an independent network. For each switching state of the converter – which is either two valve conduction or commutation – the space phasor transformation provides a subsystem in the complex plane; each of this consists of a voltage source, a grid impedance and a transformer impedance. The commutation current of each converter is derived from the imaginary part network of the respective subsystem. A generalization of the real part network leads to a generic subsystem for all switching states of the converter. A succeeding connection with a state space model of the DC network is performed; applying mesh analysis yields a differential equation system in order to derive the DC current. To verify the accuracy of the developed model, a comparison with an electromagnetic transient (EMT) model is carried out, which shows the consistence of the dynamic behavior.**

***Keywords*— Analytical Modeling, HVDC Modeling, LCC HVDC, Multiterminal HVDC, Space phasor transformation**

I. Introduction

In order to obtain an economic and reliable energy transmission grid based on decentralized renewable energy systems, the HVDC transmission becomes more and more significant, since it allows power transport over long distances with low losses. The nuclear phase-out and the reduction of CO_2 emissions in Germany leads to an expansion of renewables like solar power, onshore and offshore wind farms and biomass, which have to be integrated into the power system. The grid development plan [1] provides several HVDC interconnections to transport the electrical energy, e.g. from offshore wind farms in the north to the consumers in the south. Also in other countries like China [2] or India [3], where power transmission implies long distances from generation to the load centers, HVDC has been expanded in the last years. Beside the point-to-point interconnections, there are several studies about MT systems, which can be connected to a European Super Grid to support the existing AC grid in order to enhance the grid stability [1].

Generic root mean square (RMS) models of LCC HVDC systems as well as multiterminal configurations have already been carried out in [4] and [5]. This models can be used for power system stability studies and controller parameter calculation [6]. Analytical EMT modeling can provide a more comprehensive description of the transient behavior of line commutated converters and their interaction with the AC grid. Analytical models of LCC converters in stand-alone configuration or point-to-point interconnection were carried out in [7], so this paper is about modeling parallel and meshed MT LCC HVDC systems, which will play in important role in the future. The main advantage of the developed model is the mathematical consideration of each switching state, since frequently only steady state analysis are considered [8], [9]. Furthermore, the approach in this paper is more comprehensive than previous models, since all configurations of interconnections like point-to-point, serial, parallel and meshed systems can be regarded.

The modeling approach of this paper enables the description of a three-phase six-pulse converter as a network in the complex plane called subsystem, consisting of a voltage source and an impedance. The network elements only depend on the switching state, which is two valve conduction or commutation. To derive the subsystem, the space phasor transformation is applied and the resulting space phasor network is split in real and imaginary parts. Independently of the HVDC system configuration, the commutation current of each converter can be derived from the imaginary part network. A generalization of the real part network provides a generic model of a six-pulse converter. Connecting the subsystems subsequently with a state space model of the DC network leads to a MT HVDC model. Applying mesh analysis, a linear differential equation system can be obtained in order to derive the DC currents. The analytic model has been implemented in MATLAB®. To verify the accuracy, the simulation results are compared with an existing EMT model in SIMULINK®.

978-1-5386-2344-2/17/$31.00 ©2017 IEEE

II. MODELING OF A SIX PULSE CONVERTER

In normal operation mode, the converter has two switching states, which are two valve conduction (TVC) and commutation (COM). In the state of TVC, only two valves are conducting current simultaneously. During COM the current is redirected from one valve to another [10]. For each state, the switching conditions of the voltages and currents can be derived, which are applied in the space phasor transformation. The converter is connected to the grid through a transformer, represented by the transformer impedance Z_k, the grid can be modelled as an ideal voltage source and a grid impedance Z_{Grid}. First of all, some simplifications have to be introduced: The thyristors are regarded ideal and lossless, implying in free running state the admittance is equal to zero; in shorted state the impedance is equal to zero. The voltage sources are considered ideal and all impedances are regarded ohmic-inductive.

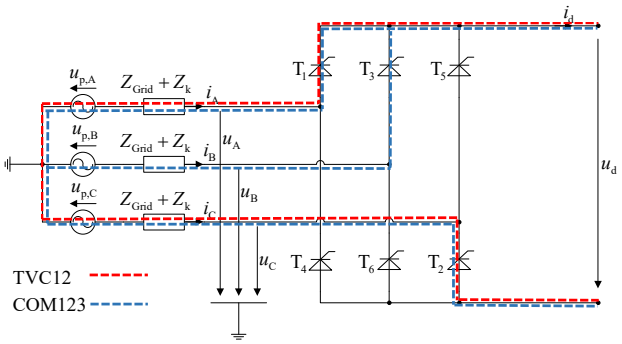

Figure 1: Line commutated six-pulse converter

To derive the space phasor network of the mentioned subsystems, the space phasor transformation is utilized [10]:

$$\underline{v} = \frac{2}{3}\left(v_A + \underline{a}v_B + \underline{a}^2 v_C\right) = \hat{V}_p \cdot e^{j\omega t}, \text{ where } \underline{a} = e^{j120°} \tag{1}$$

A. State of two valve conduction

In the state of TVC12 the valves T1 and T2 are in conducting mode and the switching conditions of the voltages and currents are defined [10]:

$$i_A = i_d,\ i_B = 0,\ i_C = -i_d,\ u_d = u_A - u_C \tag{2}$$

With the space phasor transformation (1) the space phasor for the current and the voltage reveals:

$$\underline{i}_{12} = \frac{2}{3}\left(i_A + \underline{a}i_B + \underline{a}^2 i_C\right) = \frac{2}{3}\left(1 - \underline{a}^2\right)i_d = \frac{2}{\sqrt{3}}e^{j30°} \cdot i_d \tag{3}$$

$$\begin{aligned} \underline{u}_{12} &= \frac{2}{3}\left(u_A + \underline{a}u_B + \underline{a}^2 u_C\right) = \\ &= \frac{2}{3}\left[\left(u_A - u_C\right) + e^{j120°}u_B + e^{-j60°}u_C\right] = \end{aligned} \tag{4}$$

Thus the space phasor network for TVC12 can be set up as shown in Figure 2.

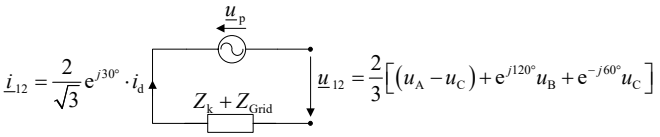

Figure 2: Space phasor network in TVC12

A rotation of -30° is applied in order to place the DC current i_d on the real axis. The current on the imaginary axis is equal to zero, so the imaginary part network is not required for the state of TVC.

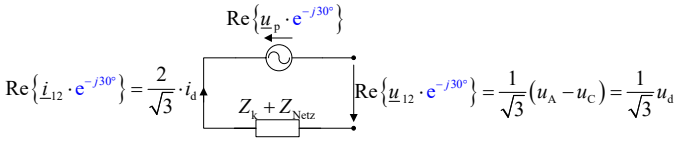

Figure 3: Real part network in TVC12

To establish the real part network for TVC in general, the rotation index z is introduced in order to describe the rotation of the phase angle of the voltage source as multiples of -30°. Multiplying the voltages in the equivalent circuit with $\sqrt{3}$ and the impedances with 2, reveals the real part network for TVC in general as shown is Figure 4.

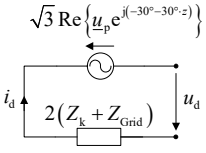

Figure 4: Real part network for TVC in general

B. State of commutation

As representation for all states of commutation the state of COM123 is now considered. The current commutates from valve T1 to T3, while T2 is still in state of conduction. To describe the state of COM the commutation current i_k is introduced, which is orthogonal to the DC current i_d in the complex plane. For the state of COM123 i_k is defined:

$$i_k = \frac{i_{T1} - i_{T3}}{2} \tag{5}$$

For the initial condition and the transition condition from COM to TVC follows:

$$i_{k,init} = \frac{1}{2}i_d,\ i_{k,trans} = -\frac{1}{2}i_d \tag{6}$$

The switching conditions of the voltages and currents during COM123 can be stated:

$$i_{T1} + i_{T2} = i_A + i_B = i_d,\ i_C = -i_d \tag{7}$$

$$u_B = u_A,\ u_A - u_C = u_d \tag{8}$$

Applying the space phasor transformation of (1) yields the appropriate voltage and current space phasors:

$$\underline{i}_{123} = \frac{2}{3}\left(i_A + \underline{a} i_B + \underline{a}^2 i_C\right) =$$
$$= \frac{2}{3}\left(\frac{1}{2}\cdot\left(i_d + 2\cdot i_k\right) + \underline{a}\cdot\frac{1}{2}\cdot\left(i_d - 2\cdot i_k\right) + \underline{a}^2\cdot\left(-i_d\right)\right) = \tag{9}$$
$$= e^{j60°}\cdot i_d + \frac{2}{\sqrt{3}}\cdot e^{-j30°}\cdot i_k$$

$$\underline{u}_{123} = \frac{2}{3}\left(u_A + \underline{a} u_B + \underline{a}^2 u_C\right) = \frac{2}{3} e^{j60°}\cdot\left(u_A - u_C\right) = \frac{2}{3}\cdot e^{j60°}\cdot u_d \tag{10}$$

With $\underline{i}_{123}$ and $\underline{u}_{123}$ the space phasor network for COM123 – which is split in real and imaginary part – can be introduced. A rotation of -60° yields that the DC current i_d lies on the real axis and the commutation current i_k lies on the imaginary axis as shown in Figure 5.

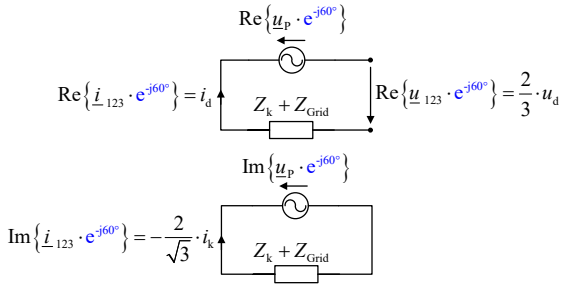

Figure 5: Real and imaginary part network in COM123

Using the rotation index z, the real and imaginary part network for the state of commutation can be derived:

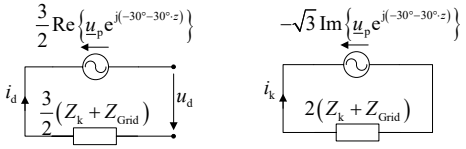

Figure 6: Real and imaginary part network for COM in general

To describe all states of TVC and COM, the rotation index z is defined in TABLE I.

TABLE I: Switching states of a six pulse converter

State	TVC12	COM123	TVC23	COM234	TVC34	COM345
z	0	1	2	3	4	5
State	TVC45	COM456	TVC56	COM561	TVC61	COM612
z	6	7	8	9	10	11

In order to calculate the commutation current $i_{k,n}$ of the n^{th} converter, the imaginary part network for COM (refer to Figure 6) is considered. $i_{k,n}$ can be derived for each converter as a result of a linear differential equation, independently of other converters in the HVDC system:

$$i_{k,n} = \left[i_{k0,n} - \frac{-\sqrt{3}\cdot\hat{u}_{p,n}}{\left|2\left(Z_{k,n} + Z_{Grid,n}\right)\right|}\cdot\sin\left(\begin{array}{c}\omega t_0 + \varphi_{Grid,n} - 30° - 30°\cdot z \\ -\arctan\left(\dfrac{X_{k,n} + X_{Grid,n}}{R_{k,n} + R_{Grid,n}}\right)\end{array}\right)\right]\cdot e^{-\frac{1}{T_{k,n}}\omega(t-t_0)} + \tag{11}$$
$$+ \frac{-\sqrt{3}\cdot\hat{u}_{p,n}}{\left|2\left(Z_{k,n} + Z_{Grid,n}\right)\right|}\cdot\sin\left(\omega t + \varphi_{Netz,n} - 30° - 30°\cdot z - \arctan\left(\frac{X_{k,n} + X_{Grid,n}}{R_{k,n} + R_{Grid,n}}\right)\right)$$

$i_{k0,n}$ is equivalent to the initial value at the point of switching, $\varphi_{Grid,n}$ refers to the grid angle and $T_{k,n}$ is defined as:

$$T_{k,n} = \frac{X_{k,n} + X_{Grid,n}}{R_{k,n} + R_{Grid,n}} \tag{12}$$

A further generalization of the real part networks in the states of TVC and COM leads to the generic network as shown in Figure 7.

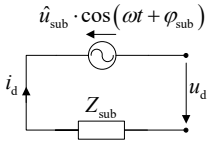

Figure 7: Generic subsystem

Each quantity in the equivalent circuit depends on the switching state or the rotation index z respectively:

$$\hat{u}_{sub} = \hat{u}_P\cdot\left[\sqrt{3}\cdot\mathrm{mod}\left(z-1;2\right) + \frac{3}{2}\cdot\mathrm{mod}\left(z;2\right)\right] \tag{13}$$

$$Z_{sub} = \left(Z_{Grid} + Z_k\right)\cdot\left[2\cdot\mathrm{mod}\left(z-1;2\right) + \frac{3}{2}\cdot\mathrm{mod}\left(z;2\right)\right] \tag{14}$$

$$\varphi_{sub} = \varphi_{Grid} - 30° - 30°\cdot z \tag{15}$$

III. Modeling of a Parallel and Meshed MT HVDC System

A model of a parallel or meshed MT HVDC system is derived by interconnecting the generic subsystems. The system shown in Figure 8 depicts a parallel 4-terminal HVDC system with two rectifiers and two inverters. The impedances refer to the grid and transformer impedances and the DC line impedances.

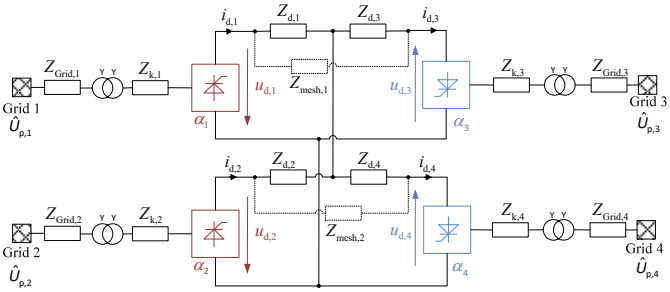

Figure 8: Configuration of a 4-terminal HVDC System

After modeling the converters as subsystems, the equivalent circuit as shown in Figure 9 can be derived (without $Z_{mesh,n}$). The impedances are composed as the sum of the DC line impedance and the impedance of a subsystem, which are depending on the switching state:

$$Z_n = Z_{sub,n} + Z_{d,n},\ n \in \{1,2,3,4\} \tag{16}$$

Once the subsystems are subsequently connected with a state space model of the DC network, the mesh currents $i_{M,n}$ can be defined, applying mesh analysis:

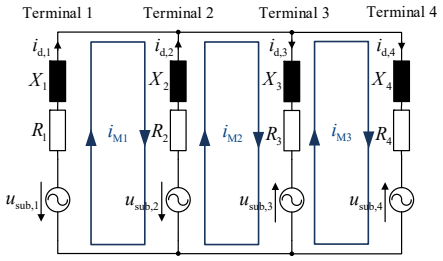

Figure 9: Radial HVDC system represented as a connection of subsystems (without $Z_{\mathrm{mesh},n}$)

For the 4-terminal HVDC system, as shown in Figure 9, the three linear independent mesh currents lead to a linear differential equation system:

$$\frac{\mathrm{d}}{\mathrm{d}\omega t}\begin{pmatrix} i_{\mathrm{M1}} \\ i_{\mathrm{M2}} \\ i_{\mathrm{M3}} \end{pmatrix} = \begin{pmatrix} X_1+X_2 & -X_2 & 0 \\ -X_2 & X_2+X_3 & -X_3 \\ 0 & -X_3 & X_3+X_4 \end{pmatrix}^{-1} \cdot \left[\begin{pmatrix} u_{\mathrm{sub},1}-u_{\mathrm{sub},2} \\ u_{\mathrm{sub},2}+u_{\mathrm{sub},3} \\ -u_{\mathrm{sub},3}+u_{\mathrm{sub},4} \end{pmatrix} - \begin{pmatrix} R_1+R_2 & -R_2 & 0 \\ -R_2 & R_2+R_3 & -R_3 \\ 0 & -R_3 & R_3+R_4 \end{pmatrix} \cdot \begin{pmatrix} i_{\mathrm{M1}} \\ i_{\mathrm{M2}} \\ i_{\mathrm{M3}} \end{pmatrix} \right]. \tag{17}$$

The solution of (17) can be expressed as the sum of a homogeneous and a specific solution:

$$\mathbf{i_M} = \mathbf{i_h} + \mathbf{i_s} \tag{18}$$

As a first step, the homogeneous solution is determined with the definition of the matrix **A**:

$$\frac{\mathrm{d}}{\mathrm{d}t}\mathbf{i_h} = \mathbf{A} \cdot \mathbf{i_h} \tag{19}$$

$$\mathbf{A} = -\begin{pmatrix} X_1+X_2 & -X_2 & 0 \\ -X_2 & X_2+X_3 & -X_3 \\ 0 & -X_3 & X_3+X_4 \end{pmatrix}^{-1} \cdot \begin{pmatrix} R_1+R_2 & -R_2 & 0 \\ -R_2 & R_2+R_3 & -R_3 \\ 0 & -R_3 & R_3+R_4 \end{pmatrix} \tag{20}$$

Using the matrix **V**, which contains the eigenvectors of matrix **A** and the eigenvalues λ_n, the homogeneous solution can be stated:

$$\mathbf{i_h} = \mathbf{V} \cdot \begin{pmatrix} \mathrm{e}^{\lambda_1 \omega t} & 0 & 0 \\ 0 & \mathrm{e}^{\lambda_2 \omega t} & 0 \\ 0 & 0 & \mathrm{e}^{\lambda_3 \omega t} \end{pmatrix} \cdot \mathbf{K} \tag{21}$$

The specific solution can be obtained by solving a equation system in the complex plane (22), resulting from mesh analysis. After a transformation from complex plane to time domain, the specific solution which describes the steady-state, can be derived (23).

$$\begin{pmatrix} \underline{\hat{I}}_{\mathrm{M1}} \\ \underline{\hat{I}}_{\mathrm{M2}} \\ \underline{\hat{I}}_{\mathrm{M3}} \end{pmatrix} = \begin{pmatrix} \underline{Z}_1+\underline{Z}_2 & -\underline{Z}_2 & 0 \\ -\underline{Z}_2 & \underline{Z}_2+\underline{Z}_3 & -\underline{Z}_3 \\ 0 & -\underline{Z}_3 & \underline{Z}_3+\underline{Z}_4 \end{pmatrix}^{-1} \cdot \begin{pmatrix} \underline{\hat{U}}_{\mathrm{sub},1}-\underline{\hat{U}}_{\mathrm{sub},2} \\ \underline{\hat{U}}_{\mathrm{sub},2}+\underline{\hat{U}}_{\mathrm{sub},3} \\ -\underline{\hat{U}}_{\mathrm{sub},3}+\underline{\hat{U}}_{\mathrm{sub},4} \end{pmatrix} \tag{22}$$

$$\mathbf{i_s} = \left|\underline{\mathbf{Z}}^{-1}\right| \cdot \hat{\mathbf{u}} \cdot \cos\left(\omega t + \boldsymbol{\varphi}_{\mathrm{u}} + \boldsymbol{\varphi}_{\mathrm{Z}}\right) \tag{23}$$

Once the homogeneous and the specific solution are determined, the matrix **K** can be derived from the initial value $t = t_0$:

$$\mathbf{i_M} = \mathbf{V} \cdot \begin{pmatrix} \mathrm{e}^{\lambda_1 \omega t} & 0 & 0 \\ 0 & \mathrm{e}^{\lambda_2 \omega t} & 0 \\ 0 & 0 & \mathrm{e}^{\lambda_3 \omega t} \end{pmatrix} \cdot \mathbf{K} + \mathbf{i_s} \tag{24}$$

$$\mathbf{K} = \left[\mathbf{V} \cdot \begin{pmatrix} \mathrm{e}^{\lambda_1 \omega t_0} & 0 & 0 \\ 0 & \mathrm{e}^{\lambda_2 \omega t_0} & 0 \\ 0 & 0 & \mathrm{e}^{\lambda_3 \omega t_0} \end{pmatrix} \right]^{-1} \cdot \left[\mathbf{i_{M0}} - \mathbf{i_s}\left(t_0\right) \right] \tag{25}$$

Afterwards, the DC currents can be deduced from the mesh currents:

$$i_{\mathrm{d},1} = i_{\mathrm{M1}},\ i_{\mathrm{d},2} = -i_{\mathrm{M1}} + i_{\mathrm{M2}},\ i_{\mathrm{d},3} = i_{\mathrm{M2}} - i_{\mathrm{M3}},\ i_{\mathrm{d},4} = i_{\mathrm{M3}} \tag{26}$$

Beside the analytical modeling of radial HVDC systems, the model can be adapted to a meshed HVDC system, as shown in Figure 10. The terminals 1 and 3 as well as the terminals 2 and 4 are exemplarily interconnected through the impedances $Z_{\mathrm{mesh},1}$ and $Z_{\mathrm{mesh},2}$ respectively. A mesh analysis leads to five linear independent mesh currents, which can be derived as previously mentioned; hence, the differential equation system can be obtained.

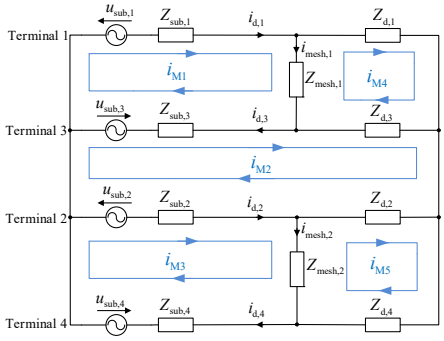

Figure 10: Mashed HVDC system represented as connection of subsystems (with $Z_{\mathrm{mesh},n}$)

For the given system configuration, the matrix A can be stated:

$$\mathbf{A} = -\begin{pmatrix} X_1+X_3+X_{\mathrm{mesh},1} & -X_3 & 0 & -X_{\mathrm{mesh}1} & 0 \\ -X_3 & X_2+X_3+X_{\mathrm{d},2}+X_{\mathrm{d},3} & -X_2 & -X_{\mathrm{d},3} & -X_{\mathrm{d},2} \\ 0 & -X_{\mathrm{sub},2} & X_2+X_4+X_{\mathrm{mesh},2} & 0 & -X_{\mathrm{mesh},2} \\ -X_{\mathrm{mesh},1} & -X_{\mathrm{d},3} & 0 & X_{\mathrm{d},1}+X_{\mathrm{d},3}+X_{\mathrm{mesh},1} & 0 \\ 0 & -Z_{\mathrm{d},2} & -X_{\mathrm{mesh},2} & 0 & X_{\mathrm{d},2}+X_{\mathrm{d},4}+X_{\mathrm{mesh},2} \end{pmatrix}^{-1} \cdot \begin{pmatrix} R_1+R_3+R_{\mathrm{mesh},1} & -R_3 & 0 & -R_{\mathrm{mesh}1} & 0 \\ -R_3 & R_2+R_3+R_{\mathrm{d},2}+R_{\mathrm{d},3} & -R_2 & -R_{\mathrm{d},3} & -R_{\mathrm{d},2} \\ 0 & -R_{\mathrm{sub},2} & R_2+R_4+R_{\mathrm{mesh},2} & 0 & -R_{\mathrm{mesh},2} \\ -R_{\mathrm{mesh},1} & -R_{\mathrm{d},3} & 0 & R_{\mathrm{d},1}+R_{\mathrm{d},3}+R_{\mathrm{mesh},1} & 0 \\ 0 & -R_{\mathrm{d},2} & -R_{\mathrm{mesh},2} & 0 & R_{\mathrm{d},2}+R_{\mathrm{d},4}+R_{\mathrm{mesh},2} \end{pmatrix} \tag{27}$$

IV. Implementation

The main part of the MATLAB® algorithm, as shown in Figure 11, is to determine the DC and commutation currents, as implemented in the first loop. For the case of TVC, the commutation current is equal to zero, during COM Eq. (11) is

applied. The second loop is responsible for the switching state changes of the converters. For the implementation of the firing angle α, the variable $t_{lz,n}$ is introduced:

$$t_{lz,n} = \left(\alpha_n - \varphi_{Grid,n} - 60°\right) \cdot \frac{T}{360°} \tag{28}$$

A transition from COM to TVC occurs, once t exceeds the length of $t_{lz,n} + T/6$. If the commutation current $i_{k,n}$ of the n^{th} subsystem is equal or less than $-i_{d,n}/2$, a transition from TVC to COM occurs. In case of changing the switching state, z is incremented, the initial values are set to the recent values and the subsystem values $\underline{\hat{u}}_{sub}$, Z_{sub} and φ_{sub} are calculated. If there is no change of switching state, the algorithm restarts. After each iteration t is incremented and once t_{calc} is reached, the simulation stops.

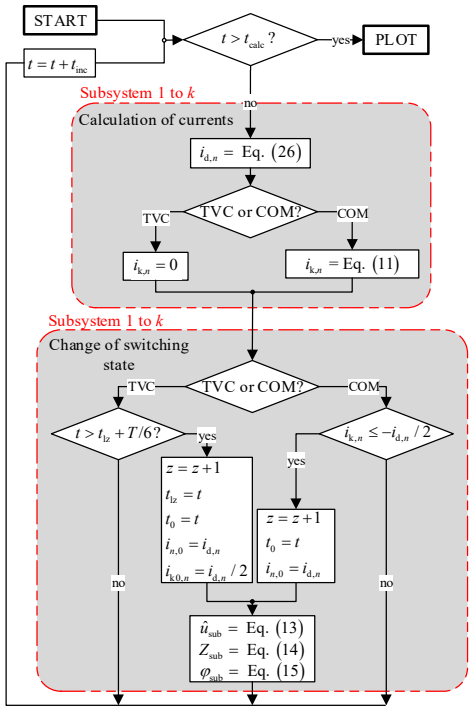

Figure 11: Flow chart of the MATLAB® algorithm

V. Results

To proof the accuracy of the developed analytical model, the simulation results are compared with an EMT model for the radial 4-terminal HVDC system as shown in Figure 8. The simulation parameters are shown in TABLE II. The simulation step size is 2 µs.

TABLE II: Parameter set of system configuration

Parameter	Terminal 1	Terminal 2	Terminal 3	Terminal 4
f [Hz]	50	50	50	50
$\underline{\hat{U}}_p$ [kV]	350	300	350	300
φ_{Grid} [°]	0	0	0	0
$\underline{Z}_d$ [Ω]	3 + j220	5 + j180	5 + j180	3 + j190
Z_{Grid} [Ω]	3.2 + j40	3+ j35	2 + j28	3 + j 39
$\underline{Z}_k$ [Ω]	2 + j20	2.1 + j24	2.2 +j 25	1,7 + j20
α [°]	35	25	122	132

The DC currents of the analytical model of each converter are shown in Figure 12, where the current flow starts at t = 7,3 ms and after 80 ms the final values are reached. In comparison, the DC currents of the EMT model, which is set up in MATLAB/Simulink® using the SimPowerSystems Toolbox, are shown in Figure 13. In order to analyze the difference between the analytical model and the EMT model in detail, the deviation δ_n (29) between both models is shown in Figure 14. It shows that the maximum deviation is about 0.3 % for δ_3 and 0.2 % for δ_4. For δ_1 and δ_2 the deviation is even less than 0.2 %, which proofs the high accuracy of the developed model.

$$\delta_n = \frac{\left|i_{d,n} - i_{d,n,EMT}\right|}{\max\left(i_{d,n,EMT}\right)} \tag{29}$$

Beside the calculation of DC currents, the algorithm determines the DC voltages of each converter, as shown in Figure 15, and the grid current space phasor as shown in Figure 16. Apart from small deviations, the DC voltages of the analytical and the EMT model are almost identical. The grid current space phasor shows the typical hexagonal shape of a six-pulse converter.

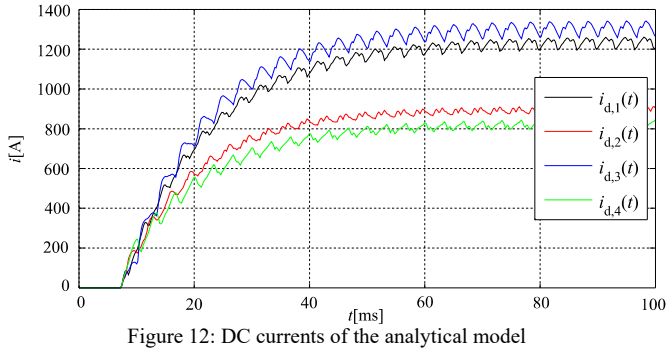

Figure 12: DC currents of the analytical model

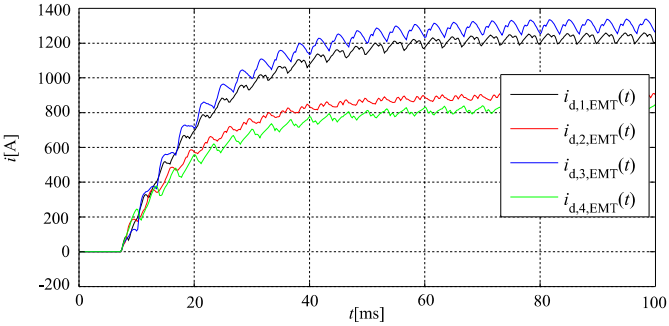

Figure 13: DC currents of the EMT Model

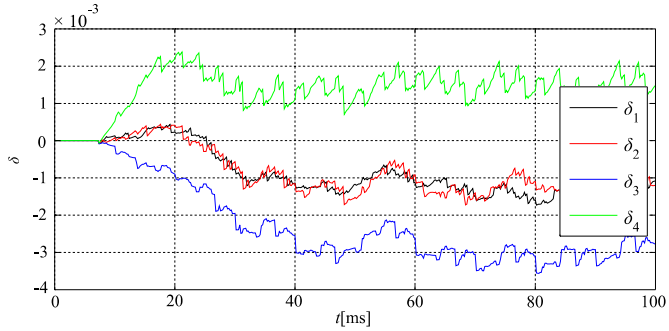

Figure 14: Deviation between the DC currents of the analytical and EMT model

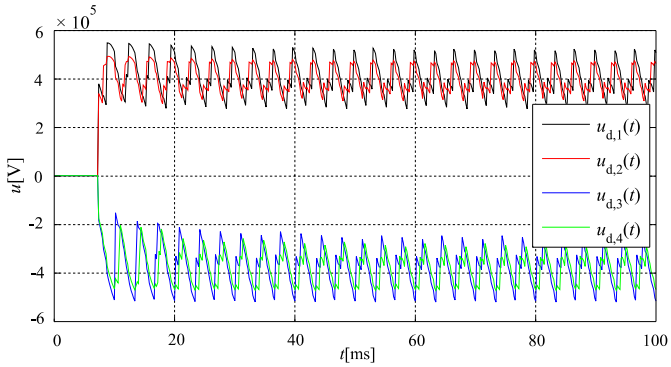

Figure 15: DC voltages of the analytical model

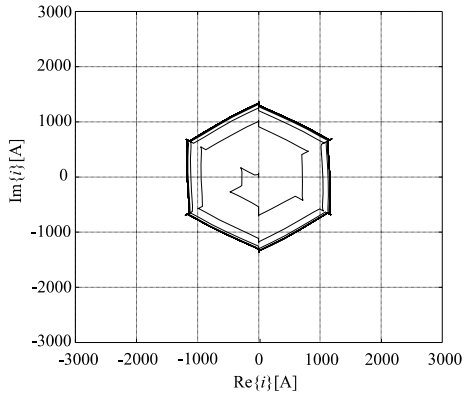

Figure 16: Grid current space phasor of terminal 1

VI. Conclusion

The developed analytical model allows a deeper insight in the operation modes and the transient behavior of LCC converters, which are interconnected to a radial or meshed MT HVDC system. The use of the space phasor transformation leads to a generic independent subsystem for each converter. The modular concept is easily expandable to a *n*-terminal system and enables the interconnection of several subsystems to radial and meshed configurations. Once the mesh currents are determined using mesh analysis, a linear differential equation system is solved in order to derive every current of the MT HVDC system. The low deviation between the DC currents of the analytical and the EMT model in a range of 0.2 % and 0.3 % proves the high accuracy of the developed model. Beside the DC currents the model provides other AC and DC quantities as well as the current and voltage space phasors of each converter. Summarized, the developed analytical model of a LCC MT HVDC system enables comprehensive transient studies, which are applicable to any *n*-terminal configuration of a HVDC system.

References

[1] 50Hz, Amprion, TenneT and TransnetBW, German grid development plan 2025 (German title: Netzentwicklungsplan Strom 2025), Berlin: German Transmission System Operators, 2015.

[2] X. Qin, P. Zeng, Q. Zhou, Q. Dai, "Study on the Development and Reliability of HVDC Transmission Systems in China", in *IEEE PES International Conference on Power System Technology* (POWERCON), Wollongong, Australia, September 2016.

[3] G. Kamalapur, V. Sheelavant, S. Hyderabad, A. Pujar, S. Baksi, A. Patil, "HVDC transmission in India", Potentials *IEEE*, vol. 33, no. 1, pp. 22-27, January 2014.

[4] C. Hahn, A. Semerow, M. Luther, O. Ruhle, "Generic Modeling of a Line Commutated HVDC System for Power System Stability Studies", in *IEEE PES Transmission & Distribution Conference & Exposition* (T&D), Chicago, USA, April 2014.

[5] C. Hahn, T. Schlegl, M. Luther, "Generic Modeling of a Line Commutated Converter based Multi-Terminal HVDC System for Power System Stability Studies", in *IEEE PES International Conference on Power System Technology* (POWERCON), Wollongong, Australia, September 2016.

[6] S. Hammer, C. Hahn, M. Luther, „Analytical Derivation of Controller Parameters for Series Connected LCC Multiterminal HVDC Systems through the use of a Decoupling Filter", in *IEEE Innovative Smart Grid Technologies Conference* (ISGT), Washington DC, USA, April 2017.

[7] L. Probst, C. Hahn, M. Luther, "A novel approach for analytical modeling of line commutated converter based HVDC systems for electromagnetic transient analysis" in *IEEE PowerTech*, Eindhoven, Netherlands, June 2015.

[8] R. Kumar, T. Leibfried, "Analytical Modelling of HVDC Transmission System Converter using Matlab/Simulink", in *IEEE Industrial and Commercial Power Systems Technical Conference*, Saratoga Springs, USA, May 2005.

[9] C. Li, X. Lin, J. Zhang, Z. Du, Y. Zhao, L. Zhao, „Analytical method for computing steady-state response of HVDC", in *IEEE Asia-Pacific Power and Energy Engineering Conference* (APPEEC), Xi'an, China, October 2016.

[10] G. Herold, *Electrical Energy Supply V: Current Converters in Three-Phase AC-Systems* (German title: Elektrische Energieverorgung V: Stromrichter in Drehstromnetzen), Wilburgstetten: Schlembach Fachverlag, 2009.

Biographies

Markus Blechschmidt received his B.Sc. and M.Sc. degree from the University of Erlangen-Nuremberg, Germany, in 2015 and 2017 respectively. His research interests lie in the field of HVDC modeling and high power converter applications.

Christoph Hahn (M'2012) received his Dipl.-Ing. degree from the University of Erlangen-Nuremberg, Germany, in 2011. Currently he is research associate and working towards a Ph.D. at the Institute of Electrical Energy Systems at the University of Erlangen-Nuremberg, Germany. His research interests lie in the field of HVDC modeling and control.

Matthias Luther (M'2011) studied electrical engineering and received his Ph.D. at the Technical University of Brunswig, Germany in 1992. From 1993 he held different functions and management positions in the electricity industry at PreussenElektra, E.ON Netz and TenneT TSO. Since 2011 he is professor and is head of the Institute of Electrical Energy Systems at the University of Erlangen-Nuremberg, Germany.